BIOCHEMISTRY
including biophysical chemistry & molecular biology

Article

pubs.acs.org/biochemistry

Efficient Stabilization of Phosphodiester (PO), Phosphorothioate (PS), and 2′-*O*-Methoxy (2′-OMe) DNA·RNA Hybrid Duplexes by Amino Sugars

I. Charles, Erik Davis, and Dev P. Arya*

Laboratory of Medicinal Chemistry, Department of Chemistry, Clemson University, Clemson, South Carolina 29634, United States

Supporting Information

ABSTRACT: Antisense strategies that target DNA·RNA hybrid structures offer potential for the development of new therapeutic drugs. The α-sarcin loop region of the 16S rRNA domain has been shown to be a high value target for such strategies. Herein, aminoglycoside interaction with three RNA·DNA α-sarcin targeted duplexes (rR·dY, rR·S-dY, and rR·2′OMe-rY) have been investigated to determine the overall effect of aminoglycoside interaction on the stability, affinity, and conformation of these hybrid duplexes. To this end, UV thermal denaturation, circular dichroism spectroscopy, fluorescence intercalator displacement, and ITC as well as DSC calorimetry experiments were carried out. The results suggest the following. (1) Of all the aminoglycosides studied, neomycin confers the highest thermal stability on all three hybrid duplexes studied. (2) There is no appreciable difference in aminoglycoside-induced thermal stability between the unmodified rR·dY and phophorothioate modified rR·S-dY duplexes. (3) The rR·2′OMe-rY duplexes thermal stability is slightly less than the other two hybrids. (4) In all three duplexes, aminoglycoside-induced thermal stability decreased as the number of amino groups decreased. (5) CD scans revealed similar spectra for the rR·dY and rR·S-dY duplexes as well as a more pronounced A-form signal for the rR·2′OMe-rY duplex. (6) FID assays paralleled the CD results, yielding similar affinity values between the rR·dY and rR·S-dY duplexes and higher affinities with the rR·2′OMe-rY duplex. (7) The overall affinity trend between aminoglycosides and the three duplexes was determined to be neomycin > paromomycin > neamine > ribostamycin. (8) ITC K_a values revealed similar binding constants for the rR·dY and rR·S-dY duplexes with rR·dY having a K_1 of $(1.03 \pm 0.58) \times 10^7$ M^{-1} and K_2 of $(1.13 \pm 0.07) \times 10^5$ M^{-1} while rR·S-dY produced a K_1 of $(1.17 \pm 0.54) \times 10^7$ M^{-1} and K_2 of $(1.27 \pm 0.69) \times 10^5$ M^{-1}. (8) The rR·2′OMe-rY produced a slightly higher binding constant values with a K_1 of $(1.25 \pm 0.24) \times 10^7$ M^{-1} and K_2 of $(3.62 \pm 0.18) \times 10^5$ M^{-1}. (9) The ΔT_m-derived K_{Tm} of 3.81×10^7 M^{-1} for rR·S-dY was in relative agreement with the corresponding K_1 of 1.17×10^7 M^{-1} derived constant from the fitted ITC. These results illustrate that the increased DNA·RNA hybrid duplex stability in the presence of aminoglycosides can help extend the roles of aminoglycosides in designing modified ODNs for targeting RNA.

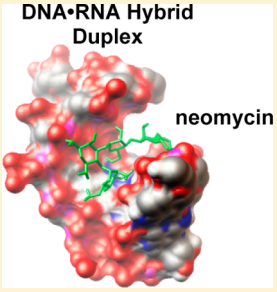

Aminoglycoside antibiotics are an important class of drugs which can be used to target specific RNA sequences. The main bactericidal activity is achieved through codon misreading after binding to the rRNA[1−6] as well as inhibition of translocation.[7,8] A variety of RNA molecules are known to interact with aminoglycosides, and they include ss RNA (poly A),[9] group I introns,[10] ribonuclease P RNA,[11] hairpin ribozyme,[12,13] hammerhead ribozyme,[14−16] hepatitis delta virus ribozyme,[17,18] untranslated region of thymidylate synthase mRNA,[6] and both Rev response element and transactivating response element RNA motifs of HIV-1.[19−21] Aminoglycoside binding to HIV-1 RNA[22,23] prevents binding of the cognate viral proteins Tat and Rev to TAR[19] and RRE,[24] respectively. Telomerase inhibition has been achieved by targeting the hTR RNA component of the enzyme via formation of an RNA·DNA hybrid.[25] The polypurine tract (PPT) of HIV and other retroviruses is essential during retroviral replication and remains as a potential target for antisense therapeutics. The RNA is digested by viral RNase H except at the polypurine tract, where an RNA·DNA hybrid resists hydrolysis and the RNA serves as a primer for the second strand DNA synthesis.[26,27]

Recently, remarkable stabilization of DNA/RNA hybrid triplexes in the presence of various aminoglycosides has been reported.[28−30] Neomycin has also been identified as the best known DNA/RNA/hybrid duplex and triplex stabilizing groove binder.[29] While DNA triple helices were significantly stabilized by neomycin, the double-helix component of the triplex formed through Watson−Crick base pairing was virtually unaffected.[28,30] Conjugation of aminoglycosides to nucleic acid binding planar moieties has been used to develop potent and selective ligands that bind to DNA·RNA hybrids,[31,32] DNA triplexes,[33−37] DNA quadruplexes,[38,39] and DNA duplexes.[40−44] As known major groove binders,[45] increased aminoglycoside binding affinity has been directly correlated with a decrease in major groove width.[46] Conversely, neomycin homodimers[47] have also been shown to exhibit high affinity for A−T-rich B-form sequences.[48] In light of the expanding platform for aminoglycoside development into new and diverse target

Received: April 13, 2012
Revised: May 26, 2012
Published: May 29, 2012

genres,[49] the path is clear for the application of effective strategies to control gene expression through the inhibition of crucial steps in translation, slicing, or activation of RNase H.[50]

Within the functionally active 16S rRNA domain, the A-site[51−55] and α-sarcin loop region are critical targets for halting protein synthesis.[56−58] The binding of aminoglycosides to the ribosomal A-site has been shown to cause an improper selection of aminoacyl-tRNA during elongation as well as translocation inhibition. A similar breakdown in ribosomal function has been linked to the α-sarcin-catalyzed hydrolysis of the phosphodiester bond that links the eighth and ninth residues within the α-sarcin loop.[59] This cleavage prevents the proper formation of elongation factor aminoacyl-tRNA complexes and results in the termination of protein synthesis.[51] The importance of this single phosphodiester linkage emphasizes the significance of the α-sarcin loop as an attractive target for antisense oligonucleotides. As such, the potential for development of novel therapeutic antisense strategies that target the α-sarcin loop is great.

The successful application of antisense oligonucleotide strategies depends upon such factors as the drug's stability toward cellular nucleases, ability to activate RNase H when hybridized to mRNA, and intracellular uptake. In order to achieve the above criteria, a variety of backbone and sugar modifications have been explored. Among them, the phosphorothioate modified S-DNA (S-dY) exhibits the most efficient intracellular uptake when compared to other modified oligonucleotides including peptide nucleic acids, 2′-*O*-methyl, and methylphosphonate oligonucleotides.[60−65] Additionally, S-DNA has been shown to activate transcription factors[66] and targets a variety of proteins such as growth factors and receptors.[67−69] Thus, phosphorothioate oligonucleotides were among the most important first generation antisense therapeutics to proceed to clinical trial stage.[70] However, the duplex stability of S-DNA with DNA and RNA has been reported to be less than its DNA counterpart.[71−76]

Our results describing aminoglycoside stabilization of hybrid duplexes[77−80] as well as neomycin assisted delivery of plasmid DNA and oligonucleotides,[81] in conjunction with the reported potential applications of S-DNA oligonucleotides in antisense therapeutics, prompted us to further explore the efficiency of aminoglycoside stabilization of phosphorothioate and 2′-*O*-methyl duplexes. Herein, we report the efficient stabilization of unmodified and modified α-sarcin mimic (rR) duplexes (rR·dY, rR·S-dY, and rR·2′OMe-rY, Scheme 1) in the presence of aminoglycosides.

Scheme 1. α-Sarcin Mimic Base Sequence (rR) as Well as the Modified and Unmodified Sequences Used To Construct rR·dY, rR·S-dY, and rR·2′OMe-rY Duplexes

rR:	3′-r(G A G A G G A)
dY:	5′-d(C T C T C C T)
S-dY:	5′-d(C*T*C*T*C*C*T) [a]
2′OMe-rY:	5′-r(CmUmCmUmCmCmUm) [b]

[a](*) indicates a phosphorothioate linkage between bases. [b](m) indicates the presence of 2′OMe groups.

MATERIALS AND METHODS

Nucleic Acids and Aminoglycosides. 7mer DNA (dY) and phosphorothioate modified DNA (S-dY) were purchased from Integrated DNA Technologies, Inc., (Coralville, IA) and were used without further purification. RNA [(rR)(2′OMe-rY)] was purchased from Dharmacon, Inc., (Lafayette, CO) and was used without further purification. Oligonucleotides used include dY, lot number 4388590; rR, lot numbers COFRA-0001 and CHAIB-0001; and S-dY, lot numbers 6928998, 6596188, and 6776459. The concentrations of all the nucleic acid solutions were determined spectrophotometrically using the following extinction coefficients (on a per strand basis, M^{-1} cm^{-1}) ε_{260} = 81 900 for rR, ε_{260} = 54 000 for S-dY, and ε_{260} = 54 000 for dY. The following aminoglycosides were purchased from ICN Pharmaceuticals, Inc. (Aurora, OH), and were used without further purification: ribostamycin (lot 98564), amikacin (lot 2775C), gentamicin (lot 93706), neomycin (lot 88235), neamine (lot 5332C), and streptomycin (lot R4235). The following were purchased from Sigma (St. Louis, MO) and were used without further purification: neomycin (lot 129H0918), paromomycin (lot 39H1276), and lividomycin (lot 77F0769). Kanamycin (lot 994856) was purchased from Fisher Scientific (Fair Lawn, NJ) and was used without further purification.

UV Spectroscopy. UV spectra were recorded at λ = 200−300 nm on a Cary 1E UV/vis spectrophotometer equipped with temperature programming. Spectrophotometer stability and λ alignment were checked prior to initiation of each melting point experiment. For accurate T_m determinations, first-derivative functions were used. Data were recorded every 1.0 deg. In all UV experiments, the samples were heated from 20 to 95 °C at a rate of 5 °C/min, annealed (95−5 °C, at a rate of 0.2 °C/min rate), and again melted (5−90 °C, at a rate of 0.2 °C/min rate), and the samples were brought back to 25 °C at a rate of 5 °C/min. During melting and annealing, the absorbance of each solution was monitored at the following wavelengths: 260, 280, and 284 nm. The second melting stage was used for calculating melting temperature.

CD Spectroscopy. All CD experiments were conducted at 15 °C on a JASCO J-810 spectrophotometer equipped with a thermoelectrically controlled cell holder. A quartz cell with a 1 cm path length was used in all CD studies. CD spectra were recorded as an average of three scans from 300 to 200 nm. In isothermal CD titration experiments, small aliquots of concentrated ligand solutions were added to 1.8 mL of 10 μM nucleic acid solutions in buffer and allowed to equilibrate for at least 20 min prior to scanning. Scanning experiments were carried out in 1.8 mL of 10 μM nucleic acid solutions in buffer without the presence of an aminoglycoside. The experiments were carried out in 60 mM total Na^+ ions, 10 mM sodium cacodylate, 0.1 mM EDTA, at pH 6.0.

FID Assays. FID experiments were conducted on a Photon Technology International (Lawrenceville, NJ) fluorimeter. The FID experiments were performed at 10 °C. The total volume used was 1.8 mL. The nucleic acid concentration used was 2 μM per duplex with a 7 μM thiazole orange (TO) concentration. The buffer used in the experiment was 10 mM sodium cacodylate, 0.1 mM EDTA, 60 mM total Na^+, and pH 6.0. TO was excited at 504 nm, and the emission was recorded from 515 to 600 nm. The ligand concentration required to displace 50% of the bound fluorescent probe was determined from a dose response curve using the Origin 5.0 software

dx.doi.org/10.1021/bi3004507 | *Biochemistry* 2012, 51, 5496−5505

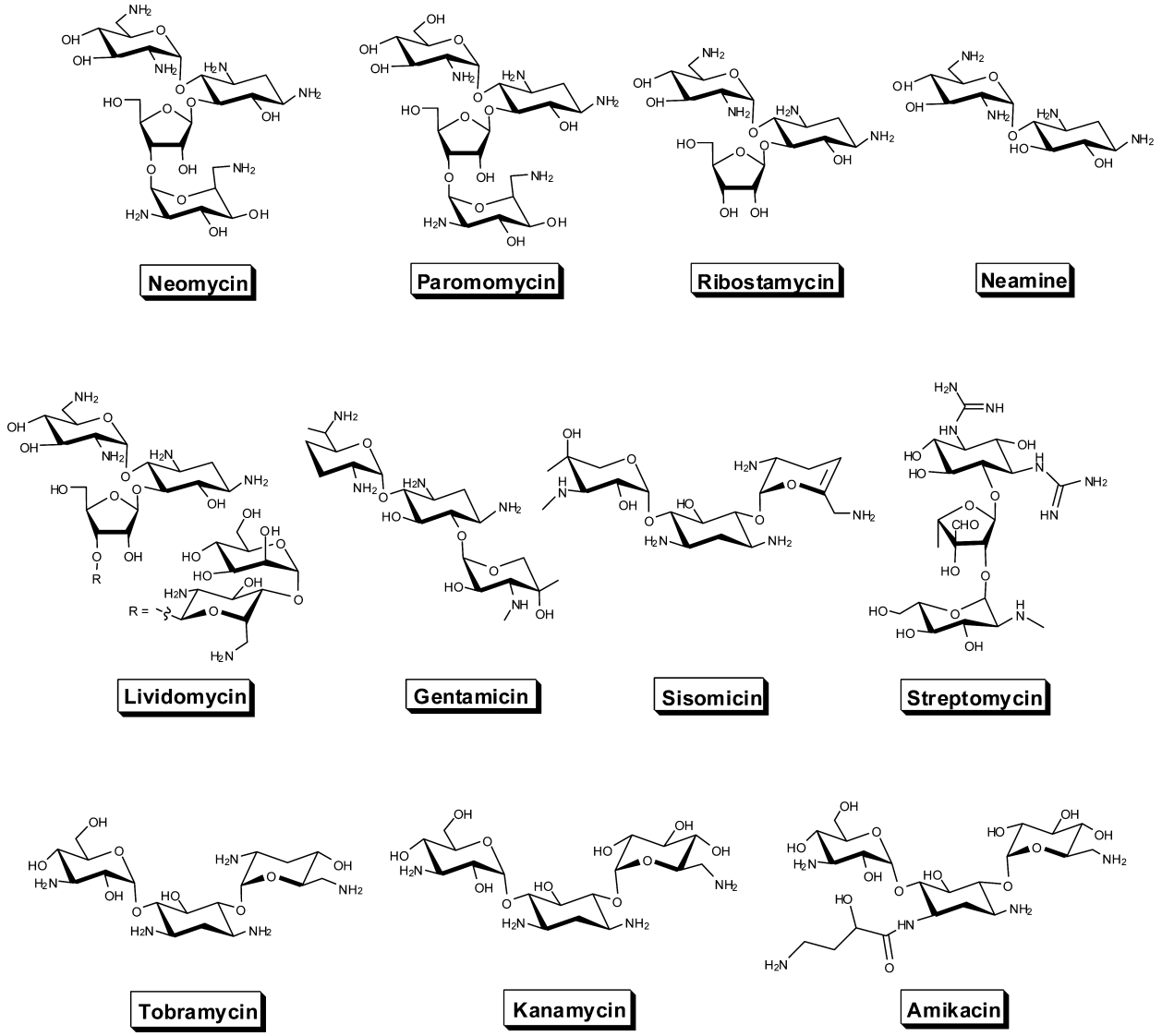

Figure 1. Chemical stuctures for the aminoglycosides studied herein.

(MicroCal, Inc., Northampton, MA) and is expressed as its AC_{50}.

ITC Studies. Isothermal titration calorimetric measurements were performed at 10 and 15 °C on a MicroCal VP-ITC (MicroCal, Inc., Northampton, MA). In a typical experiment, 5 μL aliquots of 500 μM drug were injected from a rotating syringe (300 rpm) into an isothermal sample chamber containing 1.42 mL of a duplex solution that was 20 μM per duplex. Each experiment was accompanied by control experiments in which 5 μL aliquots of the drug were titrated into buffer. The duration of each injection was 5.0 s, and the delay between each injection was 300 s. The initial delay prior to the first injection of 2 μL was 60 s. Each injection generated a heat burst curve (microcalories per second vs seconds). The area under each curve was determined by integration using Origin 5.0 software (MicroCal, Inc., Northampton, MA) to obtain a measure of the heat associated with that injection. The buffer used in the experiment was 10 mM sodium cacodylate, 0.1 mM EDTA, 60 mM total Na^+, and pH 6.0.

DSC Experiments. DSC measurements were performed using a VP-DSC Microcalorimeter from Microcal Inc. (Northampton, MA). The DSC consists of 0.511 mL of sample and reference cells. Both cells were first loaded with buffer solution, equilibrated at 5 °C for 15 min, and scanned from 5 to 90 °C at a scan rate of 60 °C/h. Extreme care was taken to minimize the presence of air bubbles in loading of the sample cell. The data were recorded every 2 s. The solution was brought back to 5 °C at the rate of 60 °C/h and incubated for 15 min. The above procedure was repeated four times in order to check for reversibility. Then, the sample cell was emptied, rinsed, and loaded with the duplex solution (40 μM per duplex) and scanned under the same conditions. The net DSC scan was analyzed for thermodynamic parameters using Origin 5.0 software (MicroCal, Inc., Northampton, MA). The pre- and post-transitional baselines were determined from least-squares fits of straight lines to the data points, respectively, below the onset of the transition peak and following the return of the transition peak to the baseline. A sigmoidal baseline was determined under the transition peak by extrapolating the pre- and post-transitional baselines and employing the profile of the transition peak. The difference in the extrapolated baselines at the transition temperature divided by the number of moles of duplex is the heat capacity change.

dx.doi.org/10.1021/bi3004507 | *Biochemistry* 2012, 51, 5496−5505

ΔT_m Method. The following equation was used to calculate association constants at the corresponding melting temperatures where the nucleic acid was complexed to the ligand.[82]

$$\frac{1}{T_m^\circ} - \frac{1}{T_m} = \frac{R}{n(\Delta H_{HS})} \ln(1 + K_{T_m} L) \quad (1)$$

T_m° is the melting temperature of ligand free nucleic acid, T_m corresponds to the melting temperature of ligand bound nucleic acid, ΔH_{HS} represents the enthalpy change corresponding to nucleic acid base pair melting in the absence of ligand (as determined by DSC measurement), L is free ligand concentration at T_m (estimated by one-half the total ligand concentration), and n is the binding site size determined by CD and fluorescence experiments. After obtaining the association constants at T_m, the integrated Van't Hoff equation (2) was used to calculate the association constants at 10 °C.[83]

$$K_{obs} = K_{T_m} / [e^{-\Delta H_{obs}/R(1/T_m - 1/T)} e^{-\Delta C_p T(1/T_m - 1/T)} (T_m/T)^{\Delta C_p/R}] \quad (2)$$

where ΔH_{obs} is the observed binding enthalpy of ligand to nucleic acid as derived from ITC excess site binding experiments at 10 °C, R is the gas constant, and ΔC_p is the heat capacity change determined from eq 3 by using binding enthalpies at various temperatures.

$$\Delta C_p = \frac{\partial H}{\partial T} \quad (3)$$

RESULTS AND DISCUSSION

UV Thermal Denaturation Studies. UV thermal denaturation of rR·dY, rR·S-dY, and rR·2′OMe-rY duplexes in the presence of various aminoglycosides was carried out in a 60 mM total sodium ion concentration (Table 1, Figure 2, Supporting Information Figures S1–S3). $\Delta T_{m2\rightarrow1}$ values were determined as the difference between the experimental and control T_m values, (Table 1, Figure 2). The results indicated that neomycin stabilized all three structures more than the other aminoglycosides studied with $\Delta T_{m2\rightarrow1}$ values of 13.7, 13.8, and 12.6 °C for the rR·dY, rR·S-dY, and rR·2′OMe-rY duplexes, respectively (Table 1, Figure 2). Paromomycin, while structurally similar, displayed lower thermal stabilization with $\Delta T_{m2\rightarrow1}$ values of 6.8, 7.8, and 4.9 °C (Table 1, Figure 2). A comparison of $\Delta T_{m2\rightarrow1}$ values for the rR·dY duplex and ribostamycin revealed 2.8 times lower thermal stability when compared to neomycin (Table 1, Figure 2). Similarly, neamine's thermal stabilization of the rR·dY duplex was 3.6 times less than neomycin (Table 1, Figure 2). Both results emphasize the importance of ring III and IV involvement in aminoglycoside–target interaction. The same pattern was observed with rR·2′OMe-rY duplex which displayed slightly lower ΔT_m values when compared to rR·dY and rR·S-dY duplexes (Table 1, Figure 2). The overall trend revealed by the ΔT_m values in Table 1 and Figure 2 reinforces the importance of amine–target electrostatic interaction with higher thermal stability being conferred by structures having more charged amines and lower thermal stabilization for ligands with fewer charged amines. This trend was found to be consistent with all three duplexes studied (Table 1, Figure 2).

The thermal denaturation value for the rR·dY duplex in the absence of aminoglycosides was found to be higher than the rR·S-dY duplex. In the presence of neomycin (r_{dup} = 1.0), the melting temperature (T_m) of rR·dY and rR·S-dY duplexes were 38 and 30 °C, respectively (Figures S1 and S2) This is in good agreement with literature where S-DNA/RNA hybrid duplexes have been shown to be thermally less stable than their unmodified counterpart.[73,74] In the presence of polyamines, phosphorothioated hybrid duplexes were reported to be thermally less stable (showing a difference in the T_m of 5

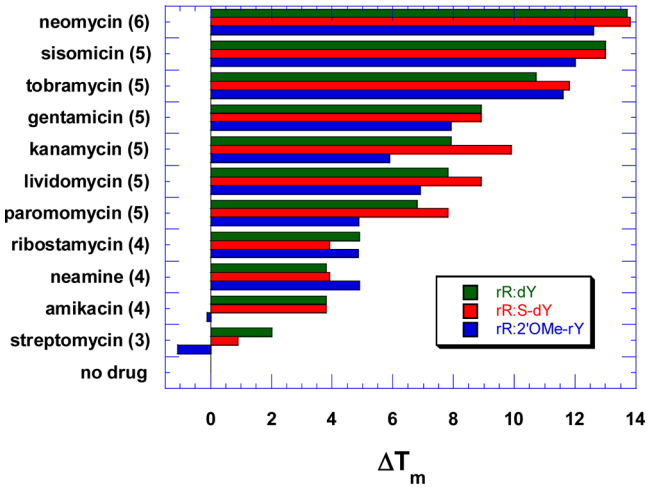

Figure 2. Change in $\Delta T_{m2\rightarrow1}$ (r_{dup} = 1.0), where r_{dup} is the ratio of the drug per duplex, derived from thermal denaturation curves for rR·dY (green), rR·S-dY (red), and rR·2′OMe-rY (blue) duplexes with various aminoglycosides. The number of possible charged amines in each ligand is listed in parentheses next to the aminoglycoside. Conditions: 10 mM sodium cacodylate, 0.1 mM EDTA, 60 mM total Na^+ ions, and pH 6.0.

Table 1. UV ΔT_m Values at 260 nm in the Presence of 60 mM Na^+ Ion Concentration with r_{dup} = 1.75[a]

	ΔT_m		
aminoglycoside	rR·dY	rR·S-dY	rR·2′OMe-rY
neomycin (6)	13.7	13.8	12.6
sisomicin (5)	13.0	13.0	12.0
tobramycin (5)	10.7	11.8	11.6
gentamicin (5)	8.9	8.9	7.9
kanamycin (5)	7.9	9.9	5.9
lividomycin (5)	7.8	8.9	6.9
paromomycin (5)	6.8	7.8	4.9
ribostamycin (4)	4.9	3.9	4.9
neamine (4)	3.8	3.9	4.9
amikacin (4)	3.8	3.8	−0.1
streptomycin (3)	2.0	0.9	−1.1

[a] r_{dup} = ratio of the drug per duplex. The number of possible charged amines for each ligand is listed in parentheses next to the aminoglycoside. Conditions: 10 mM sodium cacodylate, 0.1 mM EDTA, pH 6.0.

Table 2. AC_{50} Values Obtained From FID Assays[a]

	AC_{50} (μM)			
nucleic acid	neomycin	paromomycin	ribostamycin	neamine
rR·dY	1.0	4.2	33.6	16.5
rR·S-dY	1.1	4.3	84.3	15.9
rR·2′OMe-rY	0.44	0.83	5.3	1.3

[a] The experimental conditions are listed in the Materials and Methods section.

dx.doi.org/10.1021/bi3004507 | Biochemistry 2012, 51, 5496–5505

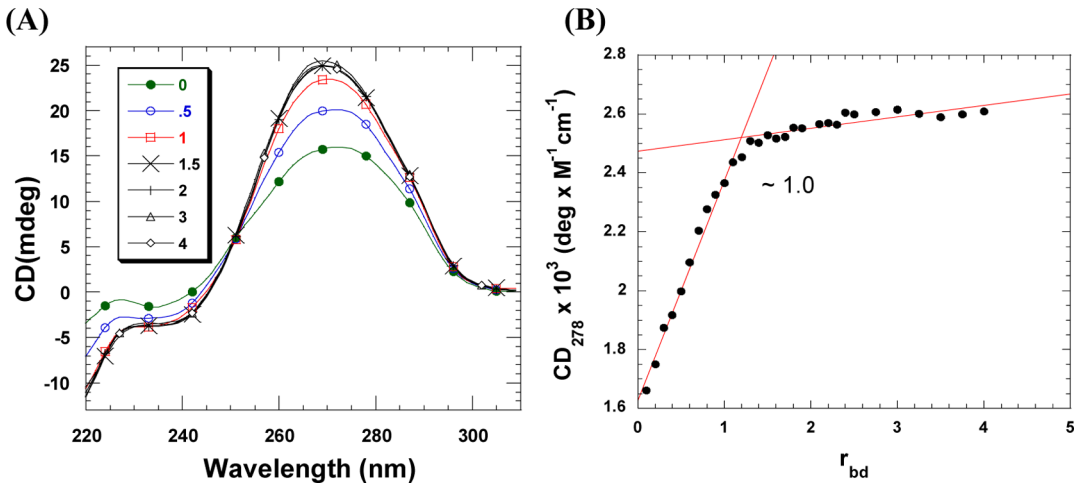

Figure 3. CD titration of 10 μM of rR·S-dY duplex with neomycin at molar ratios of 0, 0.5, 1, 1.5, 2, 3, and 4 [neomycin]/[duplex] (A). A plot of normalized molar ellipticity versus r_{dup} for CD titration of rR·S-dY duplex with neomycin (B). The continuous lines reflect the linear least-squares fits of each apparent linear domain of the experimental data (filled circles) before and after the apparent inflection points. Conditions: 10 mM sodium cacodylate, 0.1 mM EDTA, 60 mM total Na^+, pH 6.0, and 15 °C.

Table 3. Thermodynamic Binding Parameters Derived from Two-Site Model Fits of ITC-Derived Isotherms for Neomycin Titrations into the rR·dY, rR·S-dY, and rR·2′OMe-rY Duplexes[a]

nucleic acid	binding sites	N	K_a (M^{-1})	ΔH_{obs} (kcal/mol)	$T\Delta S$ (kcal/mol)	ΔG (kcal/mol)
rR·dY	2	0.4	$(1.03 \pm 0.58) \times 10^7$	−9.46 ± 0.26	−0.21	−9.25 ± 0.26
		0.3	$(1.13 \pm 0.07) \times 10^5$	−34.79 ± 0.67	−28.12	−6.67 ± 0.67
rR·S-dY	2	0.9	$(1.17 \pm 0.54) \times 10^7$	−14.88 ± 0.18	−5.55	−9.33 ± 0.18
		0.6	$(1.27 \pm 0.69) \times 10^5$	−34.09 ± 0.51	−27.35	−6.74 ± 0.51
rR·2′OMe-rY	2	0.9	$(1.25 \pm 0.24) \times 10^7$	−7.74 ± 0.08	1.61	−9.35 ± 0.08
		0.8	$(3.62 \pm 0.18) \times 10^5$	−15.01 ± 0.46	−7.68	−7.33 ± 0.46

[a]Conditions: 60 mM total Na^+ ions, 10 mM sodium cacodylate, 0.1 mM EDTA, at pH 6.0 at 15 °C.

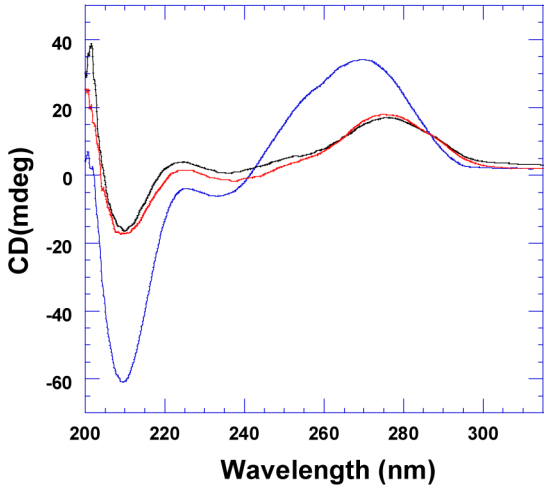

Figure 4. CD for spectra for rR·dY (black), rR·S-dY (red), and rR·2′OMe-rY (blue) duplexes 10 uM. Conditions: 60 mM total Na^+ ions, 10 mM sodium cacodylate, 0.1 mM EDTA, pH 6.0 at 15 °C.

°C) than their unmodified hybrid duplexes as well.[74] The rR·2′OMe-rY duplex, on the other hand, displayed a thermal stabilization value in the absence of an aminoglycoside that was significantly higher than either the rR·dY and rR·S-dY duplex, ΔT_m = 39 °C (Figure S3). Despite these differences, the $\Delta T_{m2\rightarrow1}$ values for all three duplexes in the presence of aminoglycosides were comparable to each other with $\Delta T_{m2\rightarrow1}$ values ±2 °C for rR·S-dY and rR·dY duplexes and slightly lower values for the rR·2′OMe-rY duplex (Table 1, Figure 2).

CD Spectroscopy. The interaction of neomycin with the rR·S-dY duplex hybrid duplex was monitored by CD spectroscopy. The CD spectrum obtained by incremental titration of neomycin into a solution of rR·S-dY duplex showed peak alterations due to the interaction between the host and ligand (Figure 3A). A plot of normalized molar ellipticity (λ = 278 nm) versus r_{dup} (Figure 3B) revealed one clear distinct inflection at 1.1 corresponding to a first binding site.

The shape of the CD spectrum changed significantly as r_{dup} was increased from 0 to 1.0 as opposed to the minimal change observed between r_{dup} 1.0 and 1.5 (Figure 3A). Further increase in r_{dup} did not alter the CD spectrum considerably (Figure 3A). This observation was found to be consistent with a binding stoichiometry of ∼1.5 neomycin molecules per duplex, which was later confirmed through ITC studies (Table 3).

CD scans were conducted to determine any structural difference between the rR·dY, rR·S-dY, and rR·2′OMe-rY duplexes (Figure 4). The CD spectra for the rR·dY and rR·S-dY duplexes were practically alike, displaying broad positive bands at 275 nm and shallow negative bands at 210 nm (Figure 4). The similarity of the spectra indicated that the phosphorothioate linkage in the rR·S-dY duplex's backbone had no appreciable effect on structure when compared to the rR·dY duplex's normal phosphodiester linkage (Figure 4). However, the rR·2′OMe-rY duplex's CD spectra showed substantial difference with an intense positive band shift at 270 nm and a strong negative band at 210 nm (Figure 4).

dx.doi.org/10.1021/bi3004507 | Biochemistry 2012, 51, 5496−5505

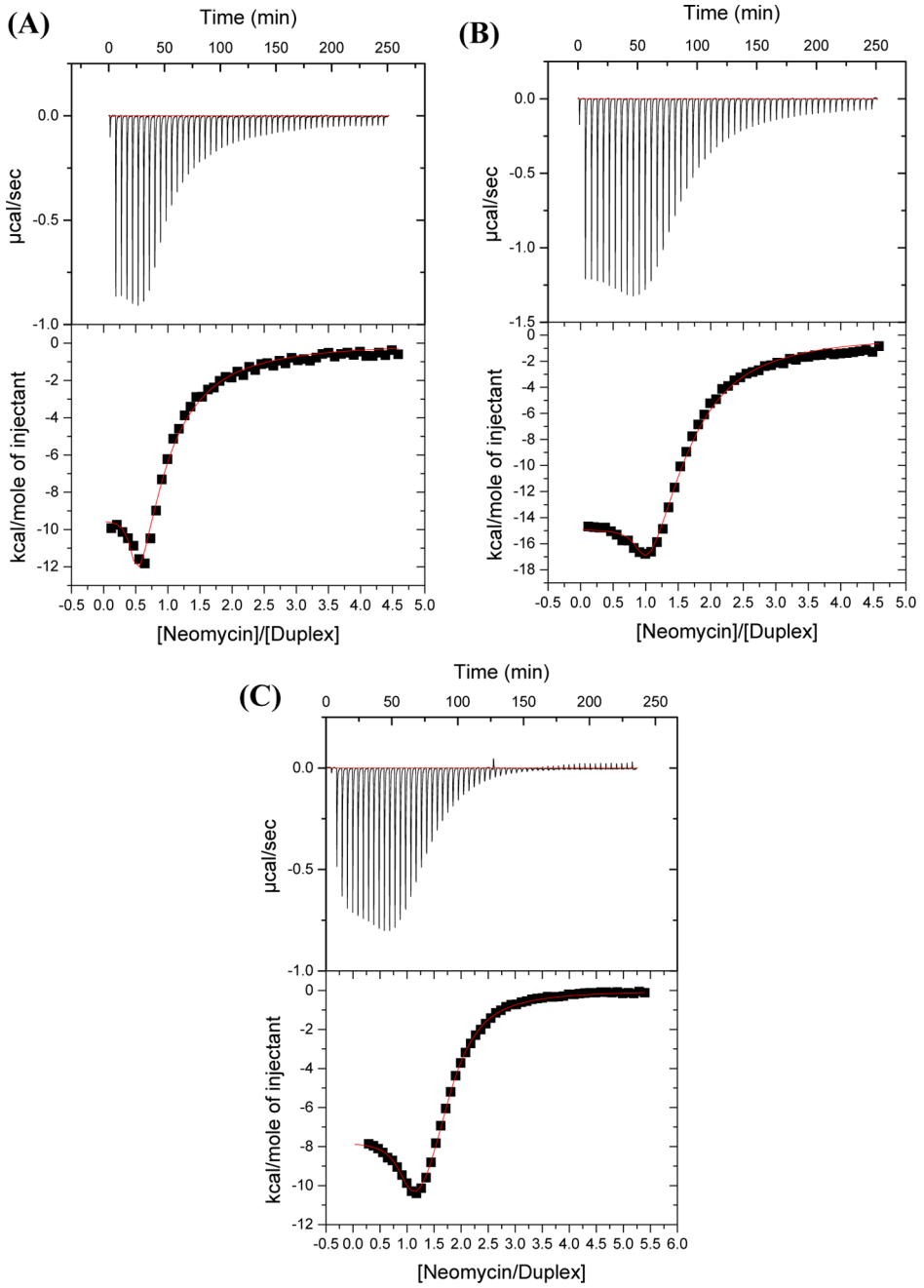

Figure 5. ITC isotherm profiles for neomycin 500 μM titrated against rR·dY (A), rR·S-dY (B), and rR·2′OMe-rY (C) duplexes, 20 μM at 15 °C. Conditions: 60 mM total Na^+ ions, 10 mM sodium cacodylate, 0.1 mM EDTA at pH 6.0.

FID Assays. FID assays were carried out to assess the overall trend for aminoglycoside binding affinity with the duplexes (Figures S4–S16). Neomycin, paromomycin, ribostamycin, and neamine were used as ligands to gauge the relative constitutive effect of charged amine and ring interaction with the targets (Figure 1). The results of these assays were compiled into Table 2 where they are represented as AC_{50} values, the concentration of ligand required to displace 50% of the intercalating fluorophore. The highest AC_{50} values were recorded with neomycin for all three duplexes (Table 2). The AC_{50} values for aminoglycoside interaction with rR·dY and rR·S-dY paralleled one another with figures that were extraordinarily close in value with an exception for rR·dY/rR·S-dY/ribostamycin interaction (Table 2). AC_{50} values for rR·2′OMe-rY were consistently lower than the values for the other two duplexes (Table 2). Both of these trends can be succinctly explained by the CD spectral differences represented in Figure 4. The rR·dY and rR·S-dY duplexes have almost identical structures and therefore parallel affinities. The rR·2′OMe-rY duplex's spectra indicates more pronounced A-form structure and hence a higher affinity. Even so, the overall trend for aminoglycosides affinity for the rR·dY, rR·S-dY, and rR·2′OMe-rY duplexes was determined to be neomycin > paromomycin > neamine > ribostamycin (Table 2).

ITC Studies. The nature of the binding of neomycin to rR·dY, rR·S-dY, and rR·2′OMe-rY duplexes was studied using ITC experiments. Figure 5 shows ITC isotherms for neomycin titrated against rR·dY, rR·S-dY, and rR·2′OMe-rY duplexes.

dx.doi.org/10.1021/bi3004507 | *Biochemistry* 2012, 51, 5496–5505

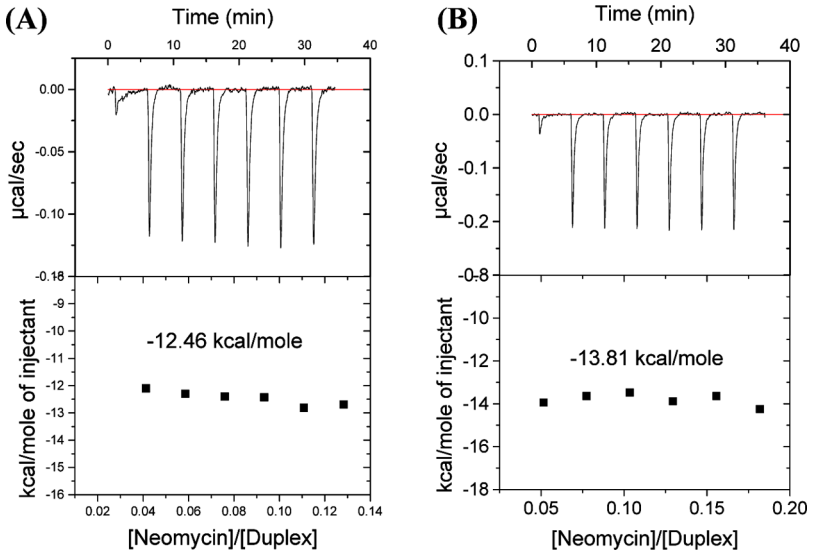

Figure 6. Excess binding site experiment: neomycin 10 μM vs rR·S-dY 50 μM at 10 °C (A). Excess binding site experiment; neomycin 10 μM vs rR·S-dY 50 μM at 15 °C (B).

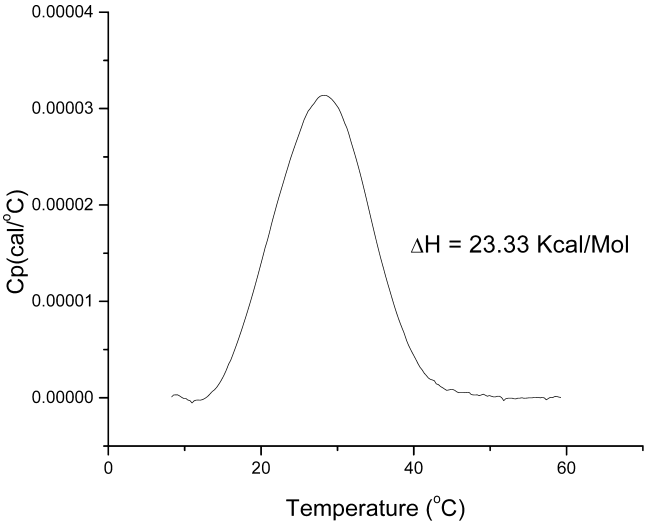

Figure 7. DSC profile of rR·S-dY duplex 40 μM per duplex. Conditions: 60 mM total Na^+ ions, 10 mM sodium cacodylate, 0.1 mM EDTA, at pH 6.0.

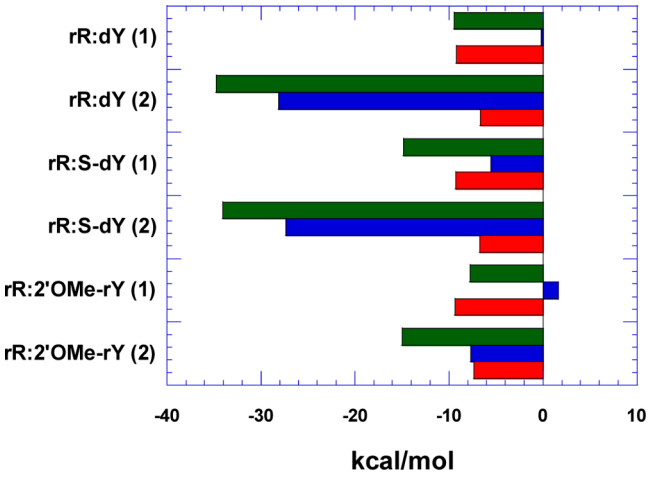

Figure 8. Thermodynamic profiles for neomycin-nucleic binding. Green bars represent ΔH values, blue bars $T\Delta S$ values, and red bars ΔG values. The number in parentheses indicates the first or second binding site for its associated duplex. Conditions: 60 mM total Na^+ ions, 10 mM sodium cacodylate, 0.1 mM EDTA, at pH 6.0 at 15 °C.

Each isotherm reveals a biphasic interaction (Figure 5). As such, all injection heat data were fitted with a model for two independent binding sites. The fits were obtained by keeping drug–duplex association constant (K_a) and observed binding enthalpy ΔH_{obs} as free-floating parameters and varying drug–duplex binding stoichiometry (N) to get less χ^2. The results are presented in the Table 3 and will be discussed in the Thermodynamic Interactions section.

DSC and ΔT_m. The ITC titration of neomycin versus rR·S-dY duplex was repeated at 10 °C in order to determine association constant (K_T) at a reference temperature (Figure 6).[84−86] The heat capacity change (ΔC_p) was calculated from ΔH_{T_1} (−13.81 kcal/mol) and ΔH_{T_2} (−12.46 kcal/mol) of the first binding event of two ITC experiments carried out at two different temperatures, T_1 (288 K) and T_2 (283 K), respectively, using eq 1 (Figure 6). The resulting calculated ΔC_p (−270 cal mol^{-1} K^{-1}) was used to estimate the apparent drug–duplex association constant at T_m from eq 2. A K_{T_m} of 5.73×10^6 M^{-1} was calculated from eq 3 using the following terms: the melting temperature of the drug-free (T_m° = 293.2 K) and drug-bound duplex (T_m = 311.04 K) (Figures S1 and S2), the enthalpy change for the melting of the duplex in the absence of bound drug (a value determined by differential scanning calorimetry, ΔH_{dup} = 23.33 kcal/mol, Figure 7), binding stoichiometry obtained from ITC experiment (n = 1.1, Figure 3), and the free drug concentration ($L = 2 \times 10^{-6}$ M) at T_m. The resulting $K_{25}^{T_m}$ of 3.81×10^7 M^{-1} was in relative agreement with the corresponding K_1 of 1.17×10^7 M^{-1} derived constant from the fitted ITC profile corroborating the result.

Thermodynamic Interactions. The results reveal two ligand binding sites for each duplex (Table 3). The binding stoichiometry for each duplex varied with a 0.7, 1.5, and 1.7 overall ligand to duplex ratio for rR·dY, rR·S-dY, and rR·2′OMe-rY respectively (Table 3). Binding constants for primary binding sites were consistently 2 orders of magnitude

dx.doi.org/10.1021/bi3004507 | Biochemistry 2012, 51, 5496−5505

higher than secondary sites (Table 3). A comparison of K_a values for rR·dY and rR·S-dY duplexes which were shown to have similar CD spectra and FID affinity (Figure 4, Table 2) revealed comparable binding constants with rR·dY having a K_1 of $(1.03 \pm 0.58) \times 10^7$ M^{-1} and K_2 of $(1.13 \pm 0.07) \times 10^5$ M^{-1} while rR·S-dY produced a K_1 of $(1.17 \pm 0.54) \times 10^7$ M^{-1} and K_2 of $(1.27 \pm 0.69) \times 10^5$ M^{-1} (Table 3). The rR·2′OMe-rY duplex whose CD spectra and FID affinity were markedly different from the other two duplexes (Figure 4, Table 2) produced slightly higher binding constant values with a K_1 of $(1.25 \pm 0.24) \times 10^7$ M^{-1} and K_2 of $(3.62 \pm 0.18) \times 10^5$ M^{-1}, which is consistent with the higher FID affinity (Tables 2 and 3).

A bar plot of the individual thermodynamic components for each hybrid duplex's interaction with neomycin according to Gibb's free energy equation is represented in Figure 8. Profiles for the rR·dY versus the rR·S-dY duplex first binding site revealed a higher negative ΔH and $T\Delta S$ for rR·S-dY when compared to rR·dY (Figure 8). However, the thermodynamic components for the second binding event in both the rR·dY and rR·S-dY duplexes were essentially the same (Figure 8). The rR·2′OMe-rY duplex first binding site produced a negative ΔH and a slightly positive $T\Delta S$ (Figure 8). The second site for rR·2′OMe-rY duplex produced a thermodynamic profile similar in character to the second site in the previous duplexes but with much lower overall negative values (Figure 8). These differences underscore the structural/conformational dissimilarities between the rR·2′OMe-rY and the rR·dY/rR·S-dY duplexes (Figures 4 and 8).

SUMMARY

While backbone-modified ODNs have shown promise as antisense therapeutic agents, the overall thermal stability of these structures can limit their potential. Herein, it has been demonstrated that aminoglycosides significantly stabilize α-sarcin loop mimic rR·dY, rR·S-dY, and rR·2′OMe-rY duplexes. Among all aminoglycosides studied, neomycin was found to be the most potent double-helix stabilizer for all three duplexes. Additionally, stabilization was demonstrated to be correlated with aminoglycoside participating amino groups and ring interactions. The structural similarities between the rR·dY and rR·S-dY duplexes produced similar binding affinities, thermodynamic profiles, and binding constants with K_a values for the PS containing rR·S-dY duplex almost equal in value to the native rR·dY species. Even though the stability of antisense phosphorothioate backbone containing oligonucleotides toward cellular nucleases, their ability to activate RNase H, and their successful intracellular uptake are better than unmodified DNA and other reported modified oligonucleotides, their thermal stability has been shown to be less than their DNA counterparts.[71−76] In this connection, our current results showing increased stability in the presence of aminoglycosides will further extend the successful application of phosphorothioate DNA and 2′OMe-DNA in antisense applications.

ASSOCIATED CONTENT

Supporting Information

Thermal denaturation plots for aminoglycoside interaction with the hybrid duplexes; FID spectra including titration plot of fluorescence intensity versus emission wavelength, maximum emission fluorescence vs addition concentration, sigmoidal curve fits, and curve fit parameter values. This material is available free of charge via the Internet at http://pubs.acs.org.

AUTHOR INFORMATION

Corresponding Author

*Tel 864-656-1106; Fax 864-656-6613; e-mail dparya@clemson.edu.

Funding

P.I. thanks the National Science Foundation (CHE/MCB-0134972) and National Institutes of Health (R41GM097917) for financial support.

Notes

The authors declare no competing financial interest.

ABBREVIATIONS

UV, ultraviolet spectroscopy; CD, circular dichroism spectroscopy; FID, fluorescence intercalator displacement; ITC, isothermal calorimetry; DSC, differential scanning calorimetry.

REFERENCES

(1) Miller, P. S., Kipp, S. A., and McGill, C. (1999) A psoralen-conjugated triplex-forming oligodeoxyribonucleotide containing alternating methylphosphonate-phosphodiester linkages: Synthesis and interactions with DNA. *Bioconjugate Chem. 10*, 572−577.

(2) Moazed, D., and Noller, H. F. (1987) Interaction of antibiotics with functional sites in 16S ribosomal RNA. *Nature 327*, 389−394.

(3) Purohit, P., and Stern, S. (1994) Interactions of a small RNA with antibiotic and RNA ligands of the 30S subunit. *Nature 370*, 659−662.

(4) Recht, M. I., Fourmy, D., Blanchard, S. C., Dahlquist, K. D., and Puglisi, J. D. (1996) RNA sequence determinants for aminoglycoside binding to an A-site rRNA model oligonucleotide. *J. Mol. Biol. 262*, 421−436.

(5) Miyaguchi, H., Narita, H., Sakamoto, K., and Yokoyama, S. (1996) An antibiotic-binding motif of an RNA fragment derived from the A-site-related region of escherichia coli 16S rRNA. *Nucleic Acids Res. 24*, 3700−3706.

(6) Tok, J. B. H., Cho, J., and Rando, R. R. (1999) Aminoglycoside antibiotics are able to specifically bind the 5′-untranslated region of thymidylate synthase messenger RNA. *Biochemistry 38*, 199−206.

(7) Davies, J., and Davis, B. D. (1968) Misreading of ribonucleic acid code words induced by aminoglycoside antibiotics. the effect of drug concentration. *J. Biol. Chem. 243*, 3312−3316.

(8) Davies, J., Gorini, L., and Davis, B. D. (1965) Misreading of RNA codewords induced by aminoglycoside antibiotics. *Mol. Pharmacol. 1*, 93−106.

(9) Xi, H., Gray, D., Kumar, S., and Arya, D. P. (2009) Molecular recognition of single-stranded RNA: Neomycin binding to poly(A). *FEBS Lett. 583*, 2269−2275.

(10) Cho, J., and Rando, R. R. (1999) Specificity in the binding of aminoglycosides to HIV-RRE RNA. *Biochemistry 38*, 8548−8554.

(11) Mikkelsen, N. E., Brannvall, M., Virtanen, A., and Kirsebom, L. A. (1999) Inhibition of RNase P RNA cleavage by aminoglycosides. *Proc. Natl. Acad. Sci. U. S. A. 96*, 6155−6160.

(12) Earnshaw, D. J., and Gait, M. J. (1998) Hairpin ribozyme cleavage catalyzed by aminoglycoside antibiotics and the polyamine spermine in the absence of metal ions. *Nucleic Acids Res. 26*, 5551−5561.

(13) Walter, F., Murchie, A. I., Thomson, J. B., and Lilley, D. M. (1998) Structure and activity of the hairpin ribozyme in its natural junction conformation: Effect of metal ions. *Biochemistry 37*, 14195−14203.

(14) Tor, Y., Hermann, T., and Westhof, E. (1998) Deciphering RNA recognition: Aminoglycoside binding to the hammerhead ribozyme. *Chem. Biol. 5*, R277−R283.

(15) Stage, T. K., Hertel, K. J., and Uhlenbeck, O. C. (1995) Inhibition of the hammerhead ribozyme by neomycin. *RNA 1*, 95−101.

(16) Clouet-d'Orval, B., Stage, T. K., and Uhlenbeck, O. C. (1995) Neomycin inhibition of the hammerhead ribozyme involves ionic interactions. *Biochemistry 34*, 11186−11190.
(17) Chia, J. S., Wu, H. L., Wang, H. W., Chen, D. S., and Chen, P. J. (1997) Inhibition of hepatitis delta virus genomic ribozyme self-cleavage by aminoglycosides. *J. Biomed. Sci. 4*, 208−216.
(18) Robles, J., and McLaughlin, L. W. (1997) DNA triplex stabilization using a tethered minor groove binding hoechst 33258 analogue. *J. Am. Chem. Soc. 119*, 6014−6021.
(19) Zapp, M. L., Stern, S., and Green, M. R. (1993) Small molecules that selectively block RNA binding of HIV-1 rev protein inhibit rev function and viral production. *Cell 74*, 969−78.
(20) Mei, H., Galan, A. A., Halim, N. S., Mack, D. P., Moreland, D. W., Sanders, K. B., Truong, H. N., and Czarnik, A. W. (1995) Inhibition of an HIV-1 tat-derived peptide binding to TAR RNA by aminoglycoside antibiotics. *Bioorg. Med. Chem. Lett. 5*, 2755−2760.
(21) Hermann, T., and Westhof, E. (1998) Saccharide-RNA recognition. *Biopolymers 48*, 155−165.
(22) Kumar, S., Kellish, P., Robinson, W. E., Wang, D., Appella, D. H., and Arya, D. P. (2012) Click dimers to target HIV TAR RNA conformation. *Biochemisry 51*, 2331−2347.
(23) Kumar, S., and Arya, D. P. (2011) Recognition of HIV TAR RNA by triazole linked neomycin dimers. *Bioorg. Med. Chem. Lett. 21*, 4788−4792.
(24) Mei, H. Y., Mack, D. P., Galan, A. A., Halim, N. S., Heldsinger, A., Loo, J. A., Moreland, D. W., Sannes-Lowery, K., Sharmeen, L., Truong, H. N., and Czarnik, A. W. (1997) Discovery of selective, small-molecule inhibitors of RNA complexes--I. the tat protein/TAR RNA complexes required for HIV-1 transcription. *Bioorg. Med. Chem. 5*, 1173−1184.
(25) Glukhov, A. I., Zimnik, O. V., Gordeev, S. A., and Severin, S. E. (1998) Inhibition of telomerase activity of melanoma cells in vitro by antisense oligonucleotides. *Biochem. Biophys. Res. Commun. 248*, 368−371.
(26) Hansen, J., Schulze, T., Mellert, W., and Moelling, K. (1988) Identification and characterization of HIV-specific RNase H by monoclonal antibody. *EMBO J. 7*, 239−243.
(27) Wohrl, B., and Moelling, K. (1990) Interaction of HIV-1 RNase H with polypurine tract containing RNA-DNA hybrids. *Biochemistry 29*, 10141−10147.
(28) Arya, D. P., and Coffee, R. L., J. (2000) DNA triple helix stabilization by aminoglycoside antibiotics. *Bioorg. Med. Chem. Lett. 10*, 1897−1899.
(29) Arya, D. P., Coffee, R. L., and Charles, I. (2001) Neomycin-induced hybrid triplex formation. *J. Am. Chem. Soc. 123*, 11093−11094.
(30) Arya, D. P., Coffee, R. L., Willis, B., and Abramovitch, A. I. (2001) Aminoglycoside-nucleic acid interactions: Remarkable stabilization of DNA and RNA triple helices by neomycin. *J. Am. Chem. Soc. 123*, 5385−5395.
(31) Shaw, N. N., and Arya, D. P. (2008) Recognition of the unique structure of DNA:RNA hybrids. *Biochimie 90*, 1026−1039.
(32) Shaw, N. N., Xi, H., and Arya, D. P. (2008) Molecular recognition of a DNA:RNA hybrid: Sub-nanomolar binding by a neomycin-methidium conjugate. *Bioorg. Med. Chem. Lett. 18*, 4142−4145.
(33) Arya, D. P., Xue, L., and Tennant, P. (2003) Combining the best in triplex recognition: Synthesis and nucleic acid binding of a BQQ-neomycin conjugate. *J. Am. Chem. Soc. 125*, 8070−8071.
(34) Arya, D. P., Xue, L., and Willis, B. (2003) Aminoglycoside (neomycin) preference is for A-form nucleic acids, not just RNA: Results from a competition dialysis study. *J. Am. Chem. Soc. 125*, 10148−10149.
(35) Xue, L., Charles, I., and Arya, D. P. (2002) Pyrene-neomycin conjugate: Dual recognition of a DNA triple helix. *Chem. Commun. 1*, 70−71.
(36) Arya, D. P., Micovic, L., Charles, I., Coffee, R. L., Jr., Willis, B., and Xue, L. (2003) Neomycin binding to watson-hoogsteen (W-H) DNA triplex groove: A model. *J. Am. Chem. Soc. 125*, 3733−3744.
(37) Xue, L., Xi, H., Kumar, S., Gray, D., Davis, E., Hamilton, P., Skriba, M., and Arya, D. P. (2010) Probing the recognition surface of a DNA triplex: Binding studies with intercalator-neomycin conjugates. *Biochemistry 49*, 5540−5552.
(38) Ranjan, N., Andreasen, K. F., Kumar, S., Hyde-Volpe, D., and Arya, D. P. (2010) Aminoglycoside binding to oxytricha nova telomeric DNA. *Biochemistry 49*, 9891−9903.
(39) Xue, L., Ranjan, N., and Arya, D. P. (2011) Synthesis and spectroscopic studies of the aminoglycoside (neomycin)-perylene conjugate binding to human telomeric DNA. *Biochemistry 50*, 2838−2849.
(40) Willis, B., and Arya, D. P. (2010) Triple recognition of B-DNA by a neomycin-hoechst 33258-pyrene conjugate. *Biochemistry 49*, 452−469.
(41) Willis, B., and Arya, D. P. (2009) Triple recognition of B-DNA. *Bioorg. Med. Chem. Lett. 19*, 4974−4979.
(42) Willis, B., and Arya, D. P. (2006) Major groove recognition of DNA by carbohydrates. *Curr. Org. Chem. 10*, 663−673.
(43) Willis, B., and Arya, D. P. (2006) Recognition of B-DNA by neomycin-hoechst 33258 conjugates. *Biochemistry 45*, 10217−10232.
(44) Arya, D. P., and Willis, B. (2003) Reaching into the major groove of B-DNA: Synthesis and nucleic acid binding of a neomycin-hoechst 33258 conjugate. *J. Am. Chem. Soc. 125*, 12398−12399.
(45) Hamilton, P. L., and Arya, D. P. (2012) Natural product DNA major groove binders. *Nat. Prod. Rep. 29*, 134−143.
(46) Xi, H., Davis, E., Ranjan, N., Xue, L., Hyde-Volpe, D., and Arya, D. P. (2011) Thermodynamics of nucleic acid "shape readout" by an aminosugar. *Biochemistry 50*, 9088−9113.
(47) Arya, D. P., Coffee, R. L., Jr., and Xue, L. (2004) From triplex to B-form duplex stabilization: Reversal of target selectivity by aminoglycoside dimers. *Bioorg. Med. Chem. Lett. 14*, 4643−4646.
(48) Kumar, S., Xue, L., and Arya, D. P. (2011) Neomycin-neomycin dimer: An all-carbohydrate scaffold with high affinity for AT-rich DNA duplexes. *J. Am. Chem. Soc. 133*, 7361−7375.
(49) Willis, B., and Arya, D. P. (2006) An expanding view of aminoglycoside-nucleic acid recognition. *Adv. Carbohydr. Chem. Biochem. 60*, 251−302.
(50) Agrawal, S., Mayrand, S. H., Zamecnik, P. C., and Pederson, T. (1990) Site-specific excision from RNA by RNase H and mixed-phosphate-backbone oligodeoxynucleotides. *Proc. Natl. Acad. Sci. U. S. A. 87*, 1401−1405.
(51) Hausner, T. P., Atmadja, J., and Nierhaus, K. H. (1987) Evidence that the G2661 region of 23S rRNA is located at the ribosomal binding sites of both elongation factors. *Biochimie 69*, 911−923.
(52) Fourmy, D., Recht, M. I., Blanchard, S. C., and Puglisi, J. D. (1996) Structure of the A site of escherichia coli 16S ribosomal RNA complexed with an aminoglycoside antibiotic. *Science 274*, 1367−1371.
(53) Fourmy, D., Recht, M. I., and Puglisi, J. D. (1998) Binding of neomycin-class aminoglycoside antibiotics to the A-site of 16 S rRNA. *J. Mol. Biol. 277*, 347−362.
(54) Fourmy, D., Yoshizawa, S., and Puglisi, J. D. (1998) Paromomycin binding induces a local conformational change in the A-site of 16 S rRNA. *J. Mol. Biol. 277*, 333−345.
(55) Carter, A. P., Clemons, W. M., Brodersen, D. E., Morgan-Warren, R., Wimberly, B. T., and Ramakrishnan, V. (2000) Functional insights from the structure of the 30S ribosomal subunit and its interactions with antibiotics. *Nature 407*, 340−348.
(56) Egebjerg, J., Larsen, N., and Garrett, R. A. (1990) *The Ribosome*, American Society For Microbiology, Washington, DC.
(57) Steitz, J. A., and Jakes, K. (1975) How ribosomes select initiator regions in mRNA: Base pair formation between the 3′ terminus of 16S rRNA and the mRNA during initiation of protein synthesis in escherichia coli. *Proc. Natl. Acad. Sci. U. S. A. 72*, 4734−4738.
(58) Hill, W. E., Camp, D. G., Tapprich, W. E., and Tassanakajohn, A. (1988) Probing ribosome structure and function using short oligodeoxyribonucleotides. *Methods Enzymol. 164*, 401−419.
(59) Endo, Y., and Wool, I. G. (1982) The site of action of alpha-sarcin on eukaryotic ribosomes. the sequence at the alpha-sarcin

cleavage site in 28 S ribosomal ribonucleic acid. *J. Biol. Chem. 257*, 9054−9060.
(60) Gray, G. D., Basu, S., and Wickstrom, E. (1997) Transformed and immortalized cellular uptake of oligodeoxynucleoside phosphorothioates, 3′-alkylamino oligodeoxynucleotides, 2′-O-methyl oligoribonucleotides, oligodeoxynucleoside methylphosphonates, and peptide nucleic acids. *Biochem. Pharmacol. 53*, 1465−1476.
(61) Iversen, P. L., Zhu, S., Meyer, A., and Zon, G. (1992) Cellular uptake and subcellular distribution of phosphorothioate oligonucleotides into cultured cells. *Antisense Res. Dev. 2*, 211−222.
(62) Crooke, R. M., Graham, M. J., Cooke, M. E., and Crooke, S. T. (1995) In vitro pharmacokinetics of phosphorothioate antisense oligonucleotides. *J. Pharmacol. Exp. Ther. 275*, 462−473.
(63) Politz, J. C., Taneja, K. L., and Singer, R. H. (1995) Characterization of hybridization between synthetic oligodeoxynucleotides and RNA in living cells. *Nucleic Acids Res. 23*, 4946−4953.
(64) Thierry, A. R., and Dritschilo, A. (1992) Intracellular availability of unmodified, phosphorothioated and liposomally encapsulated oligodeoxynucleotides for antisense activity. *Nucleic Acids Res. 20*, 5691−5698.
(65) Temsamani, J., Kubert, M., Tang, J., Padmapriya, A., and Agrawal, S. (1994) Cellular uptake of oligodeoxynucleotide phosphorothioates and their analogs. *Antisense Res. Dev. 4*, 35−42.
(66) Perez, J. R., Li, Y., Stein, C. A., Majumder, S., van Oorschot, A., and Narayanan, R. (1994) Sequence-independent induction of Sp1 transcription factor activity by phosphorothioate oligodeoxynucleotides. *Proc. Natl. Acad. Sci. U. S. A. 91*, 5957−5961.
(67) Brown, D. A., Kang, S. H., Gryaznov, S. M., DeDionisio, L., Heidenreich, O., Sullivan, S., Xu, X., and Nerenberg, M. I. (1994) Effect of phosphorothioate modification of oligodeoxynucleotides on specific protein binding. *J. Biol. Chem. 269*, 26801−26805.
(68) Khaled, Z., Benimetskaya, L., Zeltser, R., Khan, T., Sharma, H. W., Narayanan, R., and Stein, C. A. (1996) Multiple mechanisms may contribute to the cellular anti-adhesive effects of phosphorothioate oligodeoxynucleotides. *Nucleic Acids Res. 24*, 737−745.
(69) Stein, C. A. (1995) Does antisense exist? *Nat. Med. 1*, 1119−1121.
(70) Matteucci, M. D., and Wagner, R. W. (1996) In pursuit of antisense. *Nature 384*, 20−22.
(71) Clark, C. L., Cecil, P. K., Singh, D., and Gray, D. M. (1997) CD, absorption and thermodynamic analysis of repeating dinucleotide DNA, RNA and hybrid duplexes [d/r(AC)]12.[d/r(GT/U)]12 and the influence of phosphorothioate substitution. *Nucleic Acids Res. 25*, 4098−4105.
(72) Kibler-Herzog, L., Zon, G., Uznanski, B., Whittier, G., and Wilson, W. D. (1991) Duplex stabilities of phosphorothioate, methylphosphonate, and RNA analogs of two DNA 14-mers. *Nucleic Acids Res. 19*, 2979−2986.
(73) Vickers, T., Baker, B. F., Cook, P. D., Zounes, M., Buckheit, R. W., J., Germany, J., and Ecker, D. J. (1991) Inhibition of HIV-LTR gene expression by oligonucleotides targeted to the TAR element. *Nucleic Acid Res. 19*, 3359−3368.
(74) Antony, T., Thomas, T., Shirahata, A., and Thomas, T. J. (1999) Selectivity of polyamines on the stability of RNA-DNA hybrids containing phosphodiester and phosphorothioate oligodeoxyribonucleotides. *Biochemistry 38*, 10775−10784.
(75) Cummins, L., Graff, D., Beaton, G., Marshall, W. S., and Caruthers, M. H. (1996) Biochemical and physicochemical properties of phosphorodithioate DNA. *Biochemistry 35*, 8734−8741.
(76) Kandimalla, E. R., Manning, A., Zhao, Q., Shaw, D. R., Byrn, R. A., Sasisekharan, V., and Agrawal, S. (1997) Mixed backbone antisense oligonucleotides: Design, biochemical and biological properties of oligonucleotides containing 2′-5′-ribo- and 3′-5′-deoxyribonucleotide segments. *Nucleic Acid Res. 25*, 370−378.
(77) Charles, I., Xi, H., and Arya, D. P. (2007) Sequence-specific targeting of RNA with an oligonucleotide-neomycin conjugate. *Bioconjug. Chem. 18*, 160−169.
(78) Arya, D. P. (2005) Aminoglycoside-nucleic acid interactions: The case for neomycin. *Top. Curr. Chem. 253*, 149−178.
(79) Charles, I., and Arya, D. P. (2005) Synthesis of neomycin-DNA/peptide nucleic acid conjugates. *J. Carbohydr. Chem. 24*, 145−160.
(80) Charles, I., Xue, L., and Arya, D. P. (2002) Synthesis of aminoglycoside-DNA conjugates. *Bioorg. Med. Chem. Lett. 12*, 1259−1262.
(81) Napoli, S., Carbone, G. M., Catapano, C. V., Shaw, N., and Arya, D. P. (2005) Neomycin improves cationic lipid-mediated transfection of DNA in human cells. *Bioorg. Med. Chem. Lett. 15*, 3467−3469.
(82) McGhee, J. D. (1976) Theoretical calculations of the helix-coil transition of DNA in the presence of large, cooperatively binding ligands. *Biopolymers 15*, 1345−1375.
(83) Doyle, M. L., Brigham-Burke, M., Blackburn, M. N., Brooks, I. S., Smith, T. M., Newman, R., Reff, M., Stafford, W. F., III, Sweet, R. W., Truneh, A., Hensley, P., and O'Shannessy, D. J. (2000) Measurement of protein interaction bioenergetics: Application to structural variants of anti-sCD4 antibody. *Methods Enzymol. 323*, 207−230.
(84) Kaul, M., and Pilch, D. S. (2002) Thermodynamics of aminoglycoside-rRNA recognition: The binding of neomycin-class aminoglycosides to the A site of 16S rRNA. *Biochemistry 41*, 7695−7706.
(85) Haq, I., Chowdhry, B. Z., and Jenkins, T. C. (2001) Calorimetric techniques in the study of high-order DNA-drug interactions. *Methods Enzymol. 340*, 109−149.
(86) Naghibi, H., Tamura, A., and Sturtevant, J. M. (1995) Significant discrepancies between van't hoff and calorimetric enthalpies. *Proc. Natl. Acad. Sci. U. S. A. 92*, 5597−5599.